

RESEARCH OUTPUTS / RÉSULTATS DE RECHERCHE

Investigation of the Electronic Excited-State Equilibrium Geometries of Three Molecules Undergoing ESIPT

Louant, Orian; Champagne, Benoît; Liégeois, Vincent

Published in:

The Journal of physical chemistry. A, Molecules, spectroscopy, kinetics, environment, & general theory

DOI:

[10.1021/acs.jpca.7b10881](https://doi.org/10.1021/acs.jpca.7b10881)

Publication date:

2018

Document Version

Publisher's PDF, also known as Version of record

[Link to publication](#)

Citation for published version (HARVARD):

Louant, O, Champagne, B & Liégeois, V 2018, 'Investigation of the Electronic Excited-State Equilibrium Geometries of Three Molecules Undergoing ESIPT: A RI-CC2 and TDDFT Study', *The Journal of physical chemistry. A, Molecules, spectroscopy, kinetics, environment, & general theory*, vol. 122, no. 4, DOI: 10.1021/acs.jpca.7b10881, pp. 972-984. <https://doi.org/10.1021/acs.jpca.7b10881>

General rights

Copyright and moral rights for the publications made accessible in the public portal are retained by the authors and/or other copyright owners and it is a condition of accessing publications that users recognise and abide by the legal requirements associated with these rights.

- Users may download and print one copy of any publication from the public portal for the purpose of private study or research.
- You may not further distribute the material or use it for any profit-making activity or commercial gain
- You may freely distribute the URL identifying the publication in the public portal ?

Take down policy

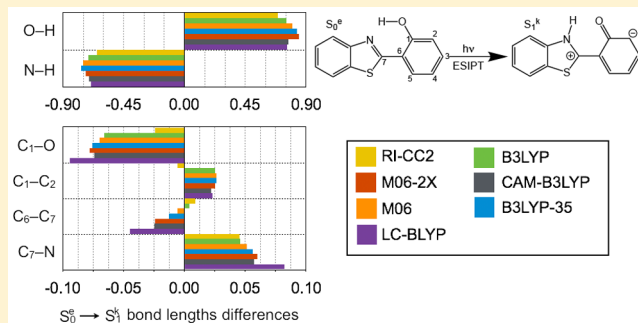
If you believe that this document breaches copyright please contact us providing details, and we will remove access to the work immediately and investigate your claim.

Investigation of the Electronic Excited-State Equilibrium Geometries of Three Molecules Undergoing ESIPT: A RI-CC2 and TDDFT Study

Orian Louant, Benoît Champagne,[✉] and Vincent Liégeois*[✉]

Laboratoire de Chimie Théorique, UCPTS, Namur Institute of Structured Matter, Université de Namur, rue de Bruxelles 61, B-5000 Namur, Belgium

ABSTRACT: Energy minima on the potential energy surfaces of the ground and excited states have been characterized for three photoactive molecules that undergo excited-state intramolecular proton transfer: 3-hydroxychromone, *N*-salicylideneaniline, and 2-(2-hydroxyphenyl)benzothiazole. Both the CC2 method and the TDDFT methodology with different exchange-correlation (XC) functionals differing by the amount of Hartree–Fock (HF) exchange have been employed. Besides the analysis of the structures along the reaction paths, this study has compared the TDDFT and CC2 results to provide guidelines for selecting the best XC functionals. Several geometrical parameters as well as the excitation energies are found to vary monotonically with the amount of HF exchange. Systematically, this study has addressed the ground-state geometries, those of the excited states, and their variations upon excitation, showing that the M06 XC functional provides the closest agreement with the CC2 results. Still, large differences of geometries have been observed between the different levels of approximation, mostly for the excited states: (i) Not all methods locate the same number of minima, (ii) the bond length variations upon excitation might be reversed, and (iii) the H-bond network can be modified from one level to another, changing the keto/enol character. Moreover, TDDFT/M06 and B3LYP-35 vertical excitation energies are in good agreement with the CC2 values. All in all, these results call for being cautious when using these optimized geometries for predicting the spectroscopic signatures of these compounds to understand the processes that take place during photoexcitation.



INTRODUCTION

Time-resolved vibrational spectroscopies such as time-resolved infrared (TRIR)¹ and femtosecond stimulated Raman spectroscopy (FSRS)² are becoming more and more widespread techniques to investigate processes taking place in electronic excited states. Among the different phenomena currently under study, we can cite excited-state intramolecular proton transfer (ESIPT) (e.g., phototautomerization),^{3–7} intermolecular charge transfer (ICT),⁸ as well as cis–trans photoisomerization.⁹ It is therefore of crucial importance to understand these processes (which involve one or more excited states) because they are involved in biochemical phenomena as well as in optoelectronic materials. Nevertheless, while these spectroscopic techniques are able to monitor the evolution of the vibrational signatures during photochemical reactions, computational methods are required to interpret the signatures in terms of atomic displacements or structural reorganizations as well as in terms of the nature of the excited states.^{5,10}

Before investigating the vibrational signatures of molecules in the excited state, an important and preliminary step consists of scanning the potential energy surface of the excited state and of characterizing their minima. While such minimization procedure is quite straightforward and reliable for ground-state structures with the use of density functional theory (DFT) combined with hybrid exchange-correlation (XC) functional,¹¹ little is known about the reliability of time-dependent density

functional theory¹² (TDDFT) and about the performance of XC functionals for describing excited-state geometries. So, even for the calculation of electronic excitation energies, for which this method is commonly used, huge variations can be found between different exchange-correlation functionals, especially for charge-transfer excitations.^{13–19} Therefore, the use of wave function theory and more specifically of high-level coupled-cluster methods²⁰ is of great interest because they form a hierarchy of approximations. Among them, the CC2 method,²¹ which is an approximation of CCSD, can be used to calculate molecular properties in the excited state for relatively quite large systems (more than 60 atoms), as illustrated by ref 22, where excitation energies have been calculated and compared with TDDFT as well as refs 23 and 24, where the excited-state polarizabilities and the excited-state dipole and quadrupole moments have been evaluated, respectively. This is made possible thanks to the use of the RI approximation.²⁵ Because analytical energy gradients have been implemented at the CC2 level for excited states, one can efficiently optimize the geometry of molecules in their excited states and use these geometries as references.

Received: November 8, 2017

Revised: December 13, 2017

Published: December 14, 2017

This work is focusing on the description of the geometrical structures for minima on the excited-state potential energy surface. For that, three photoactive molecules have been chosen owing to their rather small size and the availability of experimental data: *N*-salicylideneaniline (SaOH),^{26,27} 2-(2'-hydroxyphenyl)benzothiazole (HBT),^{10,28,29} and 3-hydroxychromone (3-HC)³⁰ (Figures 1–3). All of them display

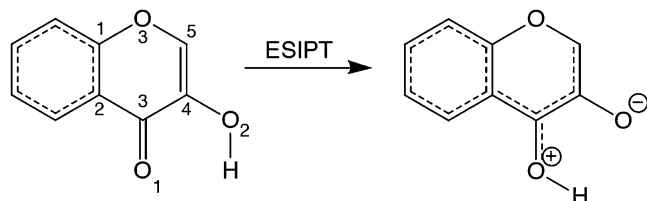


Figure 1. Structures of the ground and excited states of 3-hydroxychromone.

ESIPT phenomenon when excited at specific wavelength. First, the CC2-optimized geometries of their main excited states are described. Then, these energy minima on the potential energy surface are optimized using TDDFT with a selection of exchange-correlation functionals, differing by their percentages of Hartree–Fock exchange, and these results are compared with the CC2 reference data. The choice of the XC functionals with various percentages of HF exchange originates from the well-known impact of the HF exchange on the charge-transfer excitation energies^{13–16,19} and oscillator strengths.^{31,32} From such TDDFT versus CC2 comparisons, general rules are deduced for the choice of XC functionals. The paper is organized as follows. The second section describes the computational details. The third section presents and discusses the results. Finally, the fourth section draws conclusions and outlooks.

COMPUTATIONAL DETAILS

The geometry optimizations (ground and excited states) and calculations of vertical excitation energies at the RI-CC2 level were carried out using Turbomole 6.0.³³ The Gaussian 09³⁴ program was used for the (TD)DFT calculations with four global hybrid exchange-correlation functionals, B3LYP,³⁵ B3LYP-35 (35% HF exchange), M06, and M06-2X,³⁶ as well as two long-range-corrected hybrid functionals, LC-BLYP³⁷ and CAM-B3LYP.³⁸ These XC functionals present different percentages of Hartree–Fock exchange: 20% for B3LYP, 27% for M06, 35% for B3LYP-35, and 54% for M06-2X, while

CAM-B3LYP and LC-BLYP have 65 and 100% Hartree–Fock exchange at long-range, respectively. For all calculations, a triple- ζ basis set was used, def2-TZVPP.³⁹ For the RI-CC2 calculations, the def2-TZVPP auxiliary basis set was also used.⁴⁰ We have checked that the norm of the t2 amplitudes is <10% in all of the RI-CC2 calculations. Owing to prohibitive computational resources, no vibrational frequency calculations were performed to check the optimized geometries.

To analyze the differences of geometries, besides individual bond lengths and angles, two measures have been employed. First, the root-mean square deviation (RMSD), which, for a pair of geometries A and B (typically obtained at two levels of approximation), is defined as

$$\text{RMSD}_{A,B} = \sqrt{\frac{\sum_i^N (R_{ix}^A - R_{ix}^B)^2 + (R_{iy}^A - R_{iy}^B)^2 + (R_{iz}^A - R_{iz}^B)^2}{N}} \quad (1)$$

where R_{ix} , R_{iy} , and R_{iz} are the Cartesian coordinates of the i th atom along x , y , and z axes. The summation runs over all of the N atoms for RMSD_{tot} but only over those of the path H–O–C₁–C₆–C₇–N for RMSD_6 (used for *N*-salicylideneaniline and 2-(2'-hydroxyphenyl)benzothiazole compounds (Figures 2 and 3)). Before performing the RMSD calculations, the two structures are brought to coincide with each other by minimizing the least-squares error:^{41,42}

$$E = \frac{1}{N} \sum_i^N m_i \sum_{\alpha}^{x,y,z} \left(\sum_{\beta} \mathcal{U}_{\alpha,\beta} R_{i\beta}^A + T_{\alpha} - R_{i\alpha}^B \right)^2 \quad (2)$$

where \mathcal{U} is a 3×3 unitary rotation matrix and T is a translation vector that brings structure A to coincide with structure B. One should note that the RMSD value describes the difference between two molecular structures and is therefore not only sensitive to bond-length differences but also to differences in angles and dihedral angles.

Second, the bond length alternation (BLA) is used to describe the electron delocalization over the bonds in the “phenol” ring. According to the atom numbering of the structures (Figures 2 and 3), BLA is defined as

$$\text{BLA}_{C_1-C_6} = \frac{1}{3} [d_{12} - d_{23} + d_{34} - d_{45} + d_{56} - d_{61}] \quad (3)$$

where d_{ij} is the distance between atoms C_i and C_j . This definition assumes that BLA is positive if C₁–C₂ has a single-

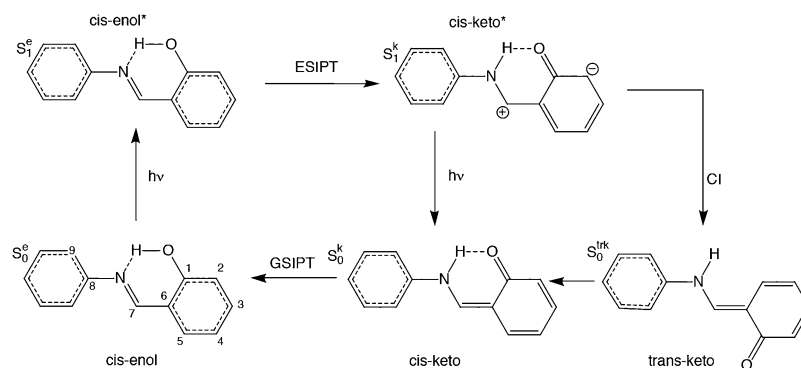


Figure 2. Structures of the ground and excited states of *N*-salicylideneaniline.

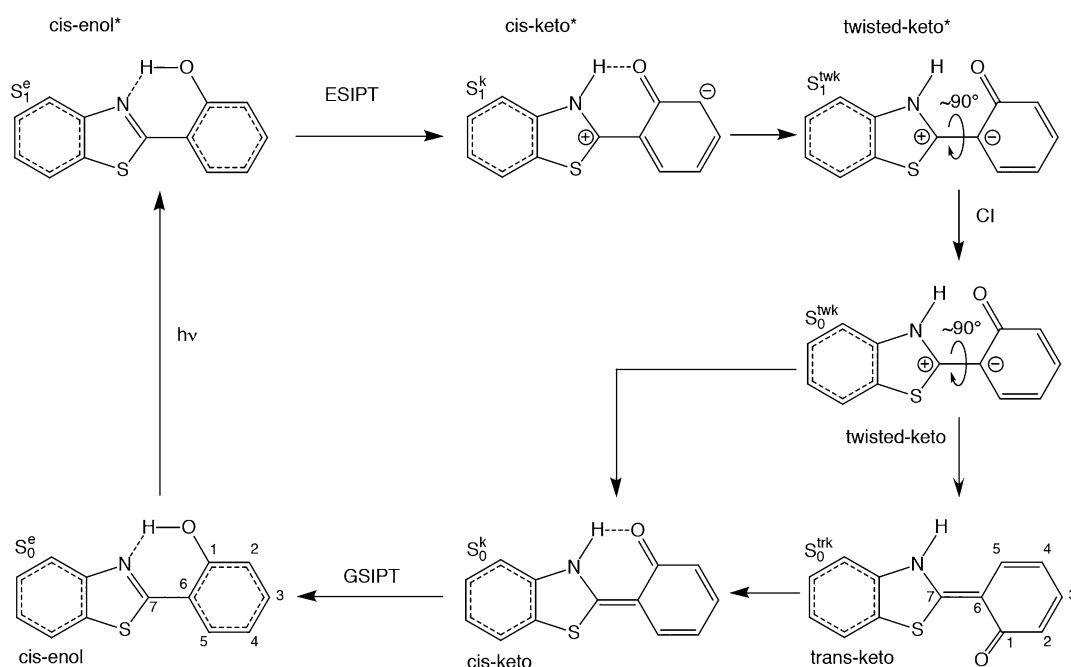


Figure 3. Representation of the ESIP process in 2-(2'-hydroxyphenyl)benzothiazole as described in ref 29, together with the structures of its ground and excited states.

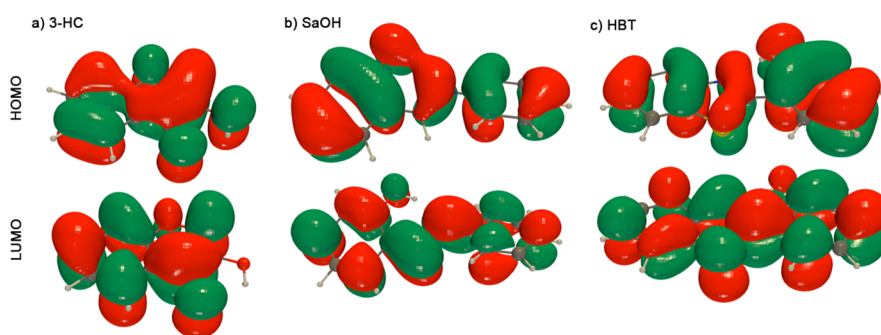


Figure 4. Representation of the HOMO and LUMO obtained at the B3LYP/def2-TZVPP level of theory of (a) 3-hydroxychromone (3-HC), (b) *N*-salicylideneaniline (SaOH), and (c) 2-(2'-hydroxyphenyl)benzothiazole (HBT).

Table 1. Excitation Energies (eV) of 3-Hydroxychromone as a Function of the Method of Calculation: Vertical Excitation Energies at Equilibrium Ground ($\Delta E_{\text{vert}}(S_0)$) and Excited ($\Delta E_{\text{vert}}(S_1)$) State Geometries as Well as Adiabatic Excitation Energies ($\Delta E_{\text{adia}}(S_0, S_1)$)

	RI-CC2	B3LYP	M06	B3LYP-35	M06-2X	CAM-B3LYP	LC-BLYP
$\Delta E_{\text{vert}}(S_0)$	4.17	3.99	4.10	4.37	4.29	4.44	4.72
$\Delta E_{\text{vert}}(S_1)$	1.54	2.21	2.38	2.51	2.73	2.52	2.79
$\Delta E_{\text{adia}}(S_0, S_1)$	2.79	3.24	3.37	3.57	3.79	3.62	4.01

bond character, C_2-C_3 is double-bond-like, and so on, and BLA is therefore negative in the opposite case. Moreover, a BLA value close to zero indicates a complete delocalization of the π electrons and therefore a very aromatic system, whereas the other situations account for quinoid character.

RESULTS AND DISCUSSION

3-Hydroxychromone. The 3-hydroxychromone molecule is sketched in Figure 1. For different definitions and levels of approximation, the $S_0 \rightarrow S_1$ excitation energies (mostly HOMO–LUMO, $\pi \rightarrow \pi^*$ transitions, Figure 4) are given in Table 1. As expected, the TDDFT vertical excitation energies increase as a function of the amount of Hartree–Fock exchange

with 3.99 and 2.21 eV for B3LYP, 4.10 and 2.38 eV for M06, 4.37 and 2.51 eV for B3LYP-35, and 4.29 (which is the exception) and 2.73 eV for M06-2X. At the ground-state equilibrium geometry, the RI-CC2 value (4.17 eV) is between the M06 and B3LYP-35 ones, while for the excited-state equilibrium geometry it is the smallest value (1.54 eV). The TDDFT adiabatic excitation energies follow the same trend as the vertical excitation energies and increase as a function of the amount of Hartree–Fock exchange. The RI-CC2 adiabatic excitation energy (2.79 eV) is the smallest value. CAM-B3LYP and LC-BLYP excitation energies are among the largest ones. Our values are in close agreement with the recent investigation of the photodynamics of 3-hydroxychromone performed by

Table 2. Representative Ground- and Excited-State Bond Lengths (Å), Valence Angles, Dihedral Angles (degrees), and RMSD Values (Å) for 3-Hydroxychromone^a

		RI-CC2	B3LYP	M06	B3LYP-35	M06-2X	CAM-B3LYP	LC-BLYP
S ₀	C ₁ –C ₂	1.402	1.401	1.395	1.395	1.394	1.392	1.380
	C ₂ –C ₃	1.451	1.459	1.453	1.460	1.460	1.456	1.449
	C ₃ –C ₄	1.447	1.459	1.454	1.458	1.460	1.456	1.450
	C ₄ –C ₅	1.356	1.347	1.343	1.340	1.341	1.338	1.326
	C ₅ –O ₃	1.358	1.356	1.348	1.352	1.352	1.352	1.345
	O ₃ –C ₁	1.362	1.358	1.348	1.354	1.352	1.352	1.343
	C ₃ –O ₁	1.249	1.231	1.223	1.222	1.221	1.223	1.214
	C ₄ –O ₂	1.349	1.349	1.338	1.324	1.346	1.344	1.338
	O ₁ –H	2.025	2.087	2.070	2.127	2.111	2.081	2.065
	O ₂ –H	0.980	0.974	0.972	0.964	0.970	0.972	0.972
	O ₁ –H–O ₂	120.1	116.7	117.0	114.2	115.7	116.3	115.8
RMSD _{tot}	—	0.017	0.015	0.026	0.021	0.017	0.025	
S ₁	C ₁ –C ₂	1.419	1.415	1.411	1.414	1.415	1.410	1.402
	C ₂ –C ₃	1.419	1.422	1.412	1.414	1.411	1.415	1.403
	C ₃ –C ₄	1.407	1.416	1.421	1.426	1.437	1.420	1.422
	C ₄ –C ₅	1.360	1.370	1.373	1.375	1.386	1.373	1.379
	C ₅ –O ₃	1.381	1.367	1.354	1.357	1.350	1.355	1.338
	O ₃ –C ₁	1.388	1.370	1.360	1.368	1.369	1.371	1.368
	C ₃ –O ₁	1.351	1.339	1.326	1.333	1.328	1.332	1.321
	C ₄ –O ₂	1.402	1.326	1.299	1.296	1.277	1.295	1.264
	O ₁ –H	0.978	0.973	0.972	0.964	0.973	0.972	0.975
	O ₂ –H	2.169	2.131	2.097	2.144	2.109	2.112	2.068
	O ₁ –H–O ₂	117.9	115.1	115.8	114.2	115.0	114.1	115.1
RMSD _{tot}	—	0.020	0.028	0.025	0.029	0.026	0.040	

^aSee Figure 1 for atom numbering. RMSD values are evaluated with respect to RI-CC2 results.

Perveaux and coworkers.⁴³ Indeed, their vertical excitation energies calculated at S₀ and S₁ geometries using PBE0/cc-pVTZ level of theory amount to 4.11 and 2.31 eV, respectively, and compare quite well with our M06/def2-TZVPP values (4.10 and 2.38 eV). They have also evaluated the CC2 vertical excitation energy at the PBE0/cc-pVTZ ground-state geometry, which amounts to 4.20 eV. This is in agreement with our RI-CC2 value of 4.17 eV calculated at the RI-CC2/def2-TZVPP ground-state geometry.

For the ground state, the optimized equilibrium geometries (Table 2) are similar to all methods, as described by small RMSD values ranging from 0.017 to 0.026 Å. The major differences are found for the positions of the O₁ atom and O₂–H group. Indeed, the C₃–O₁ bond length is systematically smaller with DFT (with values close to 1.22 Å) than using RI-CC2 (1.25 Å). For the O–H groups, the O₂–H distance is larger at the RI-CC2 level than using DFT, while the opposite is observed for the O₁–H bond. This indicates that in the ground state the intramolecular hydrogen bond is slightly stronger at the RI-CC2 level of theory than using DFT methods. One also observes a large variation of the C₄–C₅ bond length as a function of the XC functional with values ranging from 1.33 Å for LC-BLYP to 1.35 Å for B3LYP. The CC2 value attains 1.36 Å and is therefore the largest value.

The changes of geometry upon excitation are represented in Figure 5, whereas the main excited-state geometrical parameters are also listed in Table 2. The agreement between the excited-state optimized geometries at RI-CC2 and TDDFT levels is slightly poorer than for the ground state, with larger RMSD values ranging from 0.020 to 0.040 Å. Like for the ground state, the C–O distances are systematically larger with RI-CC2 than TDDFT. For instance, the C₅–O₃, O₃–C₁, and C₃–O₁ bond lengths attain 1.38, 1.39, and 1.35 Å at RI-CC2, while they

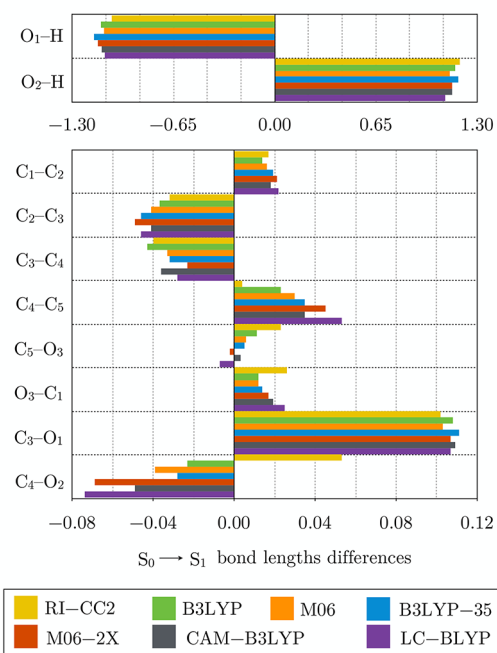


Figure 5. Bond length differences ($\Delta = d(S_1) - d(S_0)$, in Å) going from the ground state (S₀) to the excited state (S₁) of 3-hydroxychromone. See Figure 1 for atom numbering.

fluctuate around 1.36, 1.37, and 1.33 Å for the various XC functionals, respectively. On the contrary, the differences are much larger for C₄–O₂, for which RI-CC2 predicts a bond length of 1.40 Å while all XC functionals give a much smaller value, between 1.26 and 1.33 Å. Like in the ground state, the

Table 3. Difference of Energies (kJ/mol) between the Ground-State *cis*-Enol and *cis*-Keto Conformers ($\Delta E_{k-e} = E_k - E_e$) and *cis*-Enol and *trans*-Keto Conformers ($\Delta E_{trk-e} = E_{trk} - E_e$) as Well as Excitation Energies (eV) of *N*-Salicylideneaniline as a Function of the Method of Calculation: Vertical Excitation Energies at Equilibrium Ground-State Geometry of the Enol Form ($\Delta E_{vert}(S_0^e)$) and at Equilibrium Excited-State Geometry of the Keto Form ($\Delta E_{vert}(S_1^k)$) as Well as Adiabatic Excitation Energies ($\Delta E_{adia}(S_0^e, S_1^k)$)

	RI-CC2	B3LYP	M06	B3LYP-35	M06-2X	CAM-B3LYP	LC-BLYP
ΔE_{k-e}	22.9	19.4	23.6	23.6	32.7	25.0	28.4
ΔE_{trk-e}	78.2	62.3	62.7	62.3	73.2	68.3	71.2
$\Delta E_{vert}(S_0^e)$	3.85	3.67	3.76	4.01	4.14	4.12	4.51
$\Delta E_{vert}(S_1^k)$	–	2.11	2.24	2.60	2.65	2.69	3.07
$\Delta E_{adia}(S_0^e, S_1^k)$	–	2.89	3.01	3.16	3.35	3.30	3.61

O–H bond length, which is the O₁–H distance instead of the O₂–H distance in the ground state, is longer at the RI-CC2 level (0.98 Å) than at the TDDFT level (from 0.96 to 0.97 Å). Then, contrary to what was observed for the ground state, the C₄–C₅ bond length is smaller at the RI-CC2 level (1.36 Å) than using TDDFT where the value ranges from 1.37 to 1.39 Å.

Besides the O₁–H/O₂–H interchange characteristic of ESIPT, several bond length modifications are observed upon excitation (Figure 5) and can be quite different between RI-CC2 and the TDDFT methods. Among the C–C bonds, the most drastic difference is observed for the C₄–C₅ bond length, which increases by at least 0.02 Å upon excitation for all DFT/TDDFT results, while at RI-CC2 level, it only slightly increases (by 0.004 Å). In addition, the amplitude of the bond length increase is larger with the amount of HF exchange. The four C–O bond lengths increase upon excitation at the RI-CC2 level, while the C₄–O₂ bond length decreases at the DFT/TDDFT level and becomes more keto-like. The amplitudes of the C₅–O₃ bond elongation and of the C₄–O₂ bond shortening depend on the amount of HF exchange.

***N*-Salicylideneaniline.** The photodynamics of *N*-salicylideneaniline has been studied experimentally,^{26,27} and the different processes are illustrated in Figure 2. From the enol* excited state (S₁^e), the molecule undergoes an ESIPT, followed by a *cis*–*trans* isomerization to get the *trans*-keto product (S₀^{trk}), which can relax along the ground-state potential energy surface (PES) to give the *cis*-keto conformer (S₀^k) and finally the *cis*-enol conformer (S₀^e). An additional radiative pathway from the *cis*-keto conformer in the excited state (S₁^k) to the *cis*-keto conformer in the ground state (S₀^k) exists.

The difference of energy between the ground-state *cis*-enol and *cis*-keto, *trans*-keto conformers as well as the vertical excitation energies and adiabatic excitation energies at different levels of approximation are reported in Table 3. First, the differences of energy between the *cis*-keto and *cis*-enol conformations in the ground state are similar between RI-CC2 (22.9 kJ/mol) and the DFT values with the various XC functionals except for M06-2X, which predicts a much larger value at 32.7 kJ/mol. For the difference of energy between the *trans*-keto and *cis*-enol conformers, B3LYP, M06, and B3LYP-35 give roughly the same value (62.3 kJ/mol), while RI-CC2 is higher with 78.2 kJ/mol. M06-2X still has the largest value (73.2 kJ/mol) among the different XC functionals. Then, the TDDFT vertical excitation energies at the *cis*-enol ground-state equilibrium geometry (mostly HOMO–LUMO, $\pi \rightarrow \pi^*$ transitions, Figure 4) increase with the percentage of Hartree–Fock exchange from 3.67 eV for B3LYP, 3.76 eV for M06, 4.01 eV for B3LYP-35, and 4.14 eV for M06-2X, while the RI-CC2 value (3.85 eV) is between the M06 (3.76 eV) and the B3LYP-35 (4.01 eV) ones, similar to our observations for 3-

hydroxychromone. Once the *cis*-enol conformer (S₀^e) is excited, it directly undergoes the ESIPT, meaning that no equilibrium geometry was found for the S₁^e state. TDDFT with our selection of XC functionals has been able to locate a minimum in the excited state for the *cis*-keto conformers (S₁^k). On the contrary, RI-CC2 never converges to a minimum in the excited state and directly leads to the *trans*-keto product (S₀^{trk}). Indeed, after the photoexcitation and the ESIPT, we were unable to obtain a keto form at the excited state due to root flipping. When exciting from the *cis*-keto (S₀^k) form on the ground-state PES, we were too close to the conical intersection between S₀ and S₁ for RI-CC2 to optimize. Both the TDDFT vertical excitation energies at the *cis*-keto excited-state (S₁^k) equilibrium geometry and the TDDFT adiabatic excitation energies increase with the amount of Hartree–Fock exchange.

During the photodynamic (Figure 2), three ground-state minima are encountered, the *cis*-enol form (S₀^e), *cis*-keto form (S₀^k), and the *trans*-keto form (S₀^{trk}), for which representative bond lengths and angles are provided in Table 4. For the ground-state *cis*-enol form (S₀^e), we can conclude that the different methods give similar geometries because the RMSD values are small (ranging from 0.024 to 0.065 Å). However, these RMSD values are slightly larger than those of 3-hydroxychromone. This can be related to the nonplanarity of *N*-salicylideneaniline compounds with a C₇–N–C₈–C₉ torsion angle around 140°. Indeed, the largest RMSD value is observed for B3LYP, whose torsion angle (145°) deviates the most from the reference RI-CC2 value (141°). In addition, the H–O–C₁–C₆–C₇–N fragment (which is mostly planar) gives smaller RMSD than RMSD_{tot} values. Apart from the torsion angle, the major differences are found for the O–H and N–H as well as C₇–N bond lengths. RI-CC2 gives the longest O–H bond (1.00 Å) and C₇–N bond (1.30 Å) and the shortest N–H hydrogen bond (1.67 Å), indicating that the hydrogen bond is stronger with this method than with the different XC functionals. The bond-length alternations (BLAs) are all nearly identical and very close to zero, indicating that the phenol ring is aromatic with the π -electrons completely delocalized in the ring.

For the ground-state *cis*-keto form (S₀^k), the RMSD values are larger, indicating a greater difference in the geometries obtained with the various methods. One of the reasons is again the large differences in the C₇–N–C₈–C₉ torsion angle. In addition, the O–H, N–H as well as the C₁–O bond lengths vary a lot between the different methods. The O–H bond length, for instance, is the shortest with RI-CC2 (1.46 Å), while its value range from 1.65 to 1.74 Å with the different XC functionals. The O–H–N angle is also affected by the method with a value for RI-CC2 that is 10° higher than the average DFT one (150 vs 140°). There is a direct correlation between the formation of 3-

Table 4. Representative Ground-State Bond Lengths (Å), Valence Angles and Dihedral Angles (degrees), and RMSD Values (Å) for *N*-Salicylideneaniline^a

		RI-CC2	B3LYP	M06	B3LYP-35	M06-2X	CAM-B3LYP	LC-BLYP
S_0^s	C ₁ –O	1.341	1.338	1.329	1.337	1.335	1.334	1.326
	O–H	1.003	0.992	0.983	0.976	0.986	0.988	0.988
	N–H	1.672	1.744	1.786	1.798	1.761	1.744	1.731
	C ₁ –C ₂	1.398	1.397	1.392	1.393	1.395	1.392	1.385
	C ₂ –C ₃	1.387	1.384	1.378	1.380	1.381	1.378	1.368
	C ₃ –C ₄	1.400	1.398	1.392	1.393	1.395	1.392	1.385
	C ₄ –C ₅	1.384	1.381	1.375	1.378	1.379	1.375	1.367
	C ₅ –C ₆	1.405	1.404	1.398	1.400	1.399	1.397	1.387
	C ₆ –C ₁	1.417	1.418	1.410	1.411	1.410	1.408	1.396
	C ₆ –C ₇	1.438	1.446	1.442	1.450	1.452	1.448	1.445
	C ₇ –N	1.299	1.285	1.278	1.276	1.277	1.275	1.264
	O–H–N	150.2	147.4	146.1	146.0	146.6	146.9	146.3
	C ₇ –N–C ₈ –C ₉	141.0	145.1	144.0	143.1	142.1	141.0	137.9
	RMSD _{tot}	—	0.065	0.047	0.045	0.031	0.024	0.041
	RMSD ₆	—	0.024	0.038	0.041	0.030	0.025	0.024
	BLA _{C₁–C₆}	0.005	0.006	0.006	0.006	0.007	0.007	0.009
S_0^k	C ₁ –O	1.290	1.259	1.246	1.248	1.251	1.253	1.245
	O–H	1.461	1.671	1.724	1.740	1.661	1.660	1.646
	N–H	1.097	1.044	1.035	1.026	1.044	1.042	1.044
	C ₁ –C ₂	1.425	1.439	1.438	1.442	1.443	1.438	1.435
	C ₂ –C ₃	1.376	1.364	1.356	1.356	1.357	1.355	1.342
	C ₃ –C ₄	1.415	1.424	1.421	1.425	1.427	1.423	1.421
	C ₄ –C ₅	1.373	1.362	1.355	1.355	1.356	1.353	1.341
	C ₅ –C ₆	1.416	1.425	1.421	1.426	1.425	1.423	1.419
	C ₆ –C ₁	1.452	1.466	1.462	1.464	1.458	1.455	1.442
	C ₆ –C ₇	1.402	1.392	1.383	1.386	1.389	1.386	1.377
	C ₇ –N	1.323	1.326	1.323	1.324	1.320	1.318	1.309
	O–H–N	149.7	141.5	139.2	138.7	140.6	140.8	140.2
	C ₇ –N–C ₈ –C ₉	174.4	175.8	180.0	170.7	163.4	164.9	160.2
	RMSD _{tot}	—	0.065	0.114	0.109	0.177	0.155	0.216
	RMSD ₆	—	0.078	0.098	0.104	0.077	0.076	0.074
	BLA _{C₁–C₆}	0.019	0.032	0.036	0.039	0.041	0.040	0.050
S_0^{tk}	C ₁ –O	1.250	1.233	1.224	1.226	1.225	1.227	1.218
	N–H	1.010	1.008	1.008	1.001	1.008	1.007	1.007
	C ₁ –C ₂	1.452	1.459	1.455	1.460	1.464	1.458	1.455
	C ₂ –C ₃	1.364	1.354	1.348	1.347	1.347	1.345	1.332
	C ₃ –C ₄	1.430	1.435	1.431	1.436	1.441	1.437	1.437
	C ₄ –C ₅	1.365	1.356	1.349	1.349	1.348	1.346	1.332
	C ₅ –C ₆	1.426	1.433	1.428	1.435	1.438	1.434	1.432
	C ₆ –C ₁	1.479	1.488	1.480	1.483	1.480	1.477	1.465
	C ₆ –C ₇	1.379	1.375	1.367	1.369	1.368	1.365	1.352
	C ₇ –N	1.341	1.342	1.338	1.340	1.340	1.338	1.333
	C ₇ –N–C ₈ –C ₉	177.3	180.0	180.0	172.7	166.8	170.7	167.2
	RMSD _{tot}	—	0.060	0.058	0.064	0.157	0.094	0.147
	BLA _{C₁–C₆}	0.033	0.043	0.046	0.050	0.055	0.054	0.065

^aSee Figure 2 for atom numbering. RMSD values are evaluated with respect to RI-CC2 results.

the ketone (leading to a shortening of the C₁–O bond length) and the reduction of aromaticity (leading to larger BLA values). Overall, the hydrogen bond N–H···O is stronger at the RI-CC2 method than at the DFT level, while the ketone bond is stronger at the DFT level.

For the *trans*-keto ground state (S_0^{tk}), the different geometries are all very similar except for those obtained with M06-2X and LC-BLYP XC functionals. This is in correlation with the variations in the C₇–N–C₈–C₉ dihedral angle. The similarity between the structures can be explained by the absence of hydrogen bond, which was responsible for most of the differences between the structures for the *cis*-keto form. The

BLA values for each method are larger than the corresponding values for the S_0^k form (0.033 Å compared with 0.019 Å for RI-CC2). This is a consequence of the loss of the hydrogen bond in the *trans*-keto form, leading to a reduction of the aromaticity of the neighboring benzene ring. Then, the BLA values increase with the amount of Hartree–Fock exchange.

As previously said, the RI-CC2 method is not able to locate any minimum on the first excited-state PES. Then, using TDDFT, only the *cis*-keto form was found at the first excited state (S_1^k). The changes of geometry upon excitation are represented in Figure 6, whereas the main excited-state geometrical parameters are also listed in Table 5. The RMSD

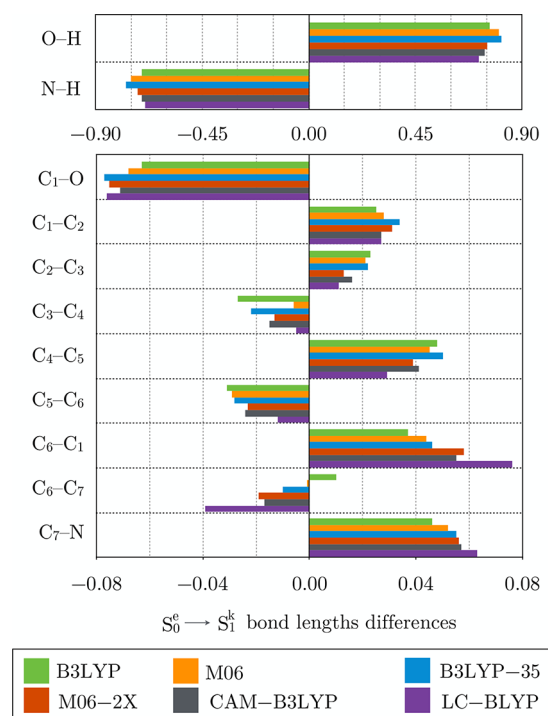


Figure 6. Bond lengths differences (in Å) going from the *cis*-enol ground state (S_0^e) to the *cis*-keto excited state (S_1^e) ($\Delta = d(S_1^e) - d(S_0^e)$) of *N*-salicylideneaniline. See Figure 2 for atom numbering.

values are relatively small except for those obtained with B3LYP-35 and LC-BLYP. The biggest difference between the geometries is due to the $C_5-C_6-C_7-N$ and $C_7-N-C_8-C_9$ torsion angles. The BLA values (Table 5) are all negative and of the same amplitude as those for the ground-state *cis*-keto form (S_0^k). Indeed, while for the excited state C_2-C_3 and C_4-C_5 are more single-like and C_3-C_4 and C_4-C_6 are double-like bonds, it is the opposite for the ground-state *cis*-keto form. For most of the geometrical changes upon excitation reported in Figure 6, the largest differences are obtained with LC-BLYP. Then, M06-2X and CAM-B3LYP values are often quite similar, while the

amplitudes of the B3LYP, M06, and B3LYP-35 geometrical changes increase, following the amount of Hartree–Fock exchange. In addition, C_6-C_7 bond-length differences (as well as C_3-C_4 ones) are strongly affected by the amount of Hartree–Fock exchange. For instance, B3LYP gives an increase in the bond length upon excitation, while M06 predicts no change and the other XC functionals predict a decrease in the distance.

2-(2'-Hydroxyphenyl)benzothiazole. The photodynamics of 2-(2'-hydroxyphenyl)benzothiazole (HBT) has been characterized in previous works, both experimentally and theoretically,^{28,29} and is illustrated in Figure 3. After photoexcitation, the *cis*-enol* undergoes an ESIP, followed by a rotation around the C–C bond. The twisted-keto* returns to the ground state through a conical intersection (CI). HBT then splits into two populations, *cis*-keto and *trans*-keto. While the first one immediately isomerizes to the *cis*-enol form, closing the proton transfer cycle, the latter requires ~ 100 ps to do so.

While experimentally four conformers are potentially observed on the ground-state PES (*cis*-enol, *trans*-keto, *cis*-keto and twisted-keto forms (Figure 3)), some of these (hypothetical) minima cannot be located by our quantum-chemistry methods. All methods were able to locate the *cis*-enol form (S_0^e), where the hydrogen is bonded to the oxygen atom as well as the *trans*-keto conformer (S_0^{tk}), but we were unable to locate the equilibrium geometry associated with the *cis*-keto conformer (S_0^k) because, experimentally, it isomerizes directly. Geometry optimization of HBT in the excited-state results in the localization of, at most, three minima, *cis*-enol* (S_1^e), *cis*-keto* (S_1^k), and twisted-keto* (S_1^{twk}), depending on the level of theory as well as on the XC functional. All TDDFT functionals locate a energy minimum close to the Franck–Condon region, which corresponds to the *cis*-enol (S_1^e). This minimum is not found at the RI-CC2 level, for which only the *cis*-keto minimum is found (S_1^k). The S_1^k minimum is also located for all of the considered XC functionals. The rotation of hydroxyphenyl group with respect to the benzothiazole conducts to a CI with the ground state at the RI-CC2 level as well as for the B3LYP and LC-BLYP XC functionals. For the other functionals, a twisted-keto minimum has been located (S_1^{twk}). Therefore,

Table 5. Representative Excited-State Bond Lengths (Å), Valence Angles and Dihedral Angles (degrees), and RMSD Values (Å) for *N*-Salicylideneaniline^a

	RI-CC2	B3LYP	M06	B3LYP-35	M06-2X	CAM-B3LYP	LC-BLYP
S_1^e							
C_1-O		1.275	1.261	1.260	1.260	1.263	1.250
$O-H$		1.756	1.784	1.790	1.739	1.731	1.707
$N-H$		1.039	1.034	1.025	1.038	1.038	1.040
C_1-C_2		1.422	1.420	1.427	1.426	1.419	1.412
C_2-C_3		1.407	1.399	1.402	1.394	1.394	1.379
C_3-C_4		1.371	1.386	1.371	1.382	1.377	1.380
C_4-C_5		1.429	1.420	1.428	1.418	1.416	1.396
C_5-C_6		1.373	1.369	1.372	1.376	1.373	1.375
C_6-C_1		1.455	1.454	1.457	1.468	1.463	1.472
C_6-C_7		1.456	1.441	1.440	1.433	1.431	1.406
C_7-N		1.331	1.330	1.331	1.333	1.332	1.327
$O-H-N$		138.0	136.7	139.8	139.3	139.8	140.4
$C_5-C_6-C_7-N$		155.8	158.1	180.0	165.2	166.8	180.0
$C_7-N-C_8-C_9$		-165.4	-166.6	-180.0	-170.1	-171.1	-180.0
$RMSD_{tot}$		–	0.038	0.193	0.082	0.094	0.193
$BLA_{C_1-C_6}$		-0.042	-0.039	-0.039	-0.032	-0.035	-0.026

^aSee Figure 2 for atom numbering. RMSD values are evaluated with respect to B3LYP results.

Table 6. Difference of Energies (kJ/mol) between the Ground-State *cis*-Enol and *trans*-Keto Conformers ($\Delta E_{\text{trk-e}} = E_{\text{trk}} - E_{\text{e}}$) as Well as Excitation Energies (eV) of 2-(2'-Hydroxyphenyl)benzothiazole as a Function of the Method of Calculation: Vertical Excitation Energies at Equilibrium Ground-State Geometry of the *cis*-Enol Form ($\Delta E_{\text{vert}}(S_0^e)$) and at Equilibrium Excited-State Geometry of the *cis*-Enol, *cis*-Keto, and Twist-Keto Form ($\Delta E_{\text{vert}}(S_1^e)$, $\Delta E_{\text{vert}}(S_1^k)$, $\Delta E_{\text{vert}}(S_1^{\text{twk}})$) State Geometries as Well as Adiabatic Excitation Energies ($\Delta E_{\text{adia}}(S_0^e, S_1^e)$, $\Delta E_{\text{adia}}(S_0^e, S_1^k)$, $\Delta E_{\text{adia}}(S_0^e, S_1^{\text{twk}})$)

	RI-CC2	B3LYP	M06	B3LYP-35	M06-2X	CAM-B3LYP	LC-BLYP
$\Delta E_{\text{trk-e}}$	83.3	74.7	76.6	79.8	89.1	81.4	85.9
$\Delta E_{\text{vert}}(S_0^e)$	3.87	3.71	3.79	4.02	4.15	4.11	4.46
$\Delta E_{\text{vert}}(S_1^e)$	–	3.23	3.40	3.54	3.40	3.58	3.75
$\Delta E_{\text{vert}}(S_1^k)$	2.29	2.51	2.58	2.71	2.68	2.87	3.12
$\Delta E_{\text{vert}}(S_1^{\text{twk}})$	–	–	0.62	0.75	0.65	0.71	–
$\Delta E_{\text{adia}}(S_0^e, S_1^e)$	–	3.50	3.59	3.77	3.86	3.83	4.10
$\Delta E_{\text{adia}}(S_0^e, S_1^k)$	3.21	3.26	3.37	3.50	3.67	3.61	3.87
$\Delta E_{\text{adia}}(S_0^e, S_1^{\text{twk}})$	–	–	2.86	3.00	3.34	3.29	–

Table 7. Representative Ground-State Bond Lengths (Å), Valence Angles and Dihedral Angles (degrees), and RMSD Values (Å) for 2-(2'-Hydroxyphenyl)benzothiazole^a

		RI-CC2	B3LYP	M06	B3LYP-35	M06-2X	CAM-B3LYP	LC-BLYP
S_0^e	C ₁ –O	1.344	1.340	1.330	1.338	1.336	1.336	1.343
	O–H	0.995	0.987	0.980	0.974	0.983	0.985	0.986
	N–H	1.703	1.750	1.782	1.788	1.763	1.743	1.727
	C ₁ –C ₂	1.399	1.398	1.394	1.395	1.397	1.394	1.386
	C ₂ –C ₃	1.386	1.382	1.375	1.378	1.379	1.375	1.366
	C ₃ –C ₄	1.399	1.397	1.392	1.393	1.395	1.392	1.385
	C ₄ –C ₅	1.384	1.380	1.374	1.376	1.377	1.374	1.365
	C ₅ –C ₆	1.404	1.404	1.398	1.401	1.399	1.397	1.388
	C ₆ –C ₁	1.417	1.418	1.411	1.412	1.410	1.408	1.396
	C ₆ –C ₇	1.446	1.453	1.449	1.456	1.458	1.455	1.452
	C ₇ –N	1.323	1.305	1.299	1.297	1.298	1.296	1.266
	C ₇ –S	1.750	1.767	1.760	1.762	1.752	1.751	1.730
	O–H–N	149.6	146.8	145.7	145.6	146.1	146.4	145.9
	C ₁ –O–H–N	0.0	0.0	0.0	0.0	0.0	0.0	0.0
	C ₅ –C ₆ –C ₇ –N	180.0	180.0	180.0	180.0	180.0	180.0	180.0
	C ₅ –C ₆ –C ₇ –S	0.0	0.0	0.0	0.0	0.0	0.0	0.0
	RMSD _{tot}	–	0.021	0.019	0.022	0.014	0.017	0.028
RMSD ₆	–	0.018	0.028	0.030	0.023	0.018	0.019	
BLA _{C₁–C₆}	0.005	0.007	0.008	0.007	0.008	0.008	0.011	
S_0^{twk}	C ₁ –O	1.279	1.251	1.241	1.241	1.240	1.244	1.235
	S–O	2.339	2.477	2.496	2.525	2.524	2.474	2.476
	N–H	1.009	1.006	1.006	0.999	1.006	1.005	1.006
	C ₁ –C ₂	1.428	1.443	1.440	1.445	1.449	1.442	1.440
	C ₂ –C ₃	1.376	1.362	1.355	1.355	1.355	1.353	1.340
	C ₃ –C ₄	1.415	1.423	1.419	1.424	1.428	1.423	1.423
	C ₄ –C ₅	1.376	1.364	1.357	1.357	1.357	1.355	1.341
	C ₅ –C ₆	1.412	1.422	1.417	1.423	1.424	1.420	1.418
	C ₆ –C ₁	1.444	1.458	1.453	1.456	1.455	1.448	1.436
	C ₆ –C ₇	1.402	1.397	1.390	1.392	1.393	1.391	1.381
	C ₇ –N	1.356	1.357	1.352	1.354	1.353	1.351	1.343
	C ₇ –S	1.729	1.742	1.735	1.740	1.734	1.731	1.717
	C ₁ –O–H–N	0.0	0.0	0.0	0.0	0.0	0.0	0.0
	C ₅ –C ₆ –C ₇ –N	0.0	0.0	0.0	0.0	0.0	0.0	0.0
	C ₅ –C ₆ –C ₇ –S	179.8	180.0	180.0	180.0	180.0	180.0	180.0
	RMSD _{tot}	–	0.051	0.060	0.068	0.067	0.051	0.060
	BLA _{C₁–C₆}	0.020	0.034	0.037	0.042	0.045	0.043	0.055

^aSee Figure 3 for atom numbering. RMSD values are evaluated with respect to RI-CC2 results.

while RI-CC2 locates only one minimum on the first excited-state PES (S_1^k), TDDFT functionals locate a second minimum (S_1^e) and even a third one (S_1^{twk}) with the M06, B3LYP-35, M06-2X, and CAM-B3LYP functionals.

The energy differences between the *trans*-keto and *cis*-enol ground-state equilibrium structures are reported in Table 6 together with the vertical excitation energies of the first dipole-allowed transition (mostly HOMO–LUMO, $\pi \rightarrow \pi^*$ transitions, Figure 4). For the first set of values, RI-CC2 one

(83.3 kJ/mol) is among the highest values together with M06-2X (89.1 kJ/mol) and LC-BLYP (85.9 kJ/mol). For the vertical excitation energies, the TDDFT results show a clear trend: The excitation energies go up as a function of the percentage of Hartree–Fock exchange for hybrid functionals with 3.71, 3.23, and 2.51 eV for B3LYP, 3.79, 3.40, and 2.58 eV for M06, 4.02, 3.54, and 2.71 eV for B3LYP-35, and 4.15, 3.40, and 2.68 eV for M06-2X. Regarding the long-range corrected hybrid functionals, CAM-B3LYP (4.11, 3.58, and 2.87 eV) and LC-BLYP (4.46, 3.75, and 3.12 eV) present higher excitation energy values than most of the other functionals. The RI-CC2 vertical excitation energy at the *cis*-enol equilibrium geometry (3.87 eV) is between the M06 and B3LYP-35 values, as already found for the two previous molecules. For the adiabatic energies, they also increase with the amount of Hartree–Fock exchange when going from B3LYP to M06-2X, while the LC-BLYP values are the largest ones.

Some representative geometrical parameters of the *cis*-enol (S_0^e) and *trans*-keto (S_0^{tk}) conformers are given in Table 7. From the root-mean-square deviations (RMSDs), it appears that the changes are rather small and slightly larger for the *trans*-keto form (maximum 0.028 Å for S_0^e and maximum 0.067 Å for S_0^{tk}). For the *cis*-enol form, the major discrepancies are found for the C_1 –O, C_7 –N, O–H, and N–H bond lengths. Indeed, the first three bonds are longer at the RI-CC2 level (1.34, 1.00, 1.32 Å), while the N–H bond (1.70 Å) is smaller compared with those obtained at the DFT level. This indicates once more that the hydrogen bond is stronger at the RI-CC2 level of theory. For the *trans*-keto form, the most drastic change of bond length is observed for the double-bond C_1 –O, which is maximum for the RI-CC2 method (1.28 Å) and slightly decreases with the amount of Hartree–Fock exchange in the XC functionals (from 1.25 Å for B3LYP to 1.24 Å for M06-2X), together with an increase in the S–O distance from 2.34 Å for RI-CC2 to 2.48 Å for B3LYP and 2.53 Å for B3LYP-35. The BLAs for the *cis*-enol ground state are close to 0.007 Å (compared to 0.000 Å for benzene), while its values for the *trans*-keto ground state range from 0.020 to 0.055 Å, which indicates a reduction of the aromaticity with the loss of the hydrogen bond, as already shown for the *N*-salicylideneaniline molecule.

The geometrical changes upon the $S_0^e \rightarrow S_1^e$ transition are represented in Figure 7a, while selected excited-state bond lengths, valence angles, and dihedral angles are tabulated in Table 8. We were not able to locate the S_1^e minimum at the RI-CC2 level of theory because this method directly follows the ES IPT reaction to form the S_1^k product. Therefore, the RMSD values measure the difference of geometry with respect to the B3LYP one. With respect to the S_0^e , the S_1^e minimum presents (Figure 7a) a reduced C_1 –O bond length, while the O–H bond length increases. In parallel, the O–H–N angle increases, leading to an important reduction of the N–H distance. This reduction of the N–H distance is accompanied by an increase in the C_7 –N bond length. While the changes in the C_1 –O distances are similar for all XC functionals, bigger differences are observed for O–H and N–H, suggesting that the S_1^e minimum is an intermediate between the enol and keto compounds. The RMSD values between the different XC functionals further evidence that while the deviations are still rather small, they are larger than in the ground state and are mainly due to differences in the O–H and N–H bond lengths. B3LYP is the functional that presents the most significant increase in the O–H distance and an equally important

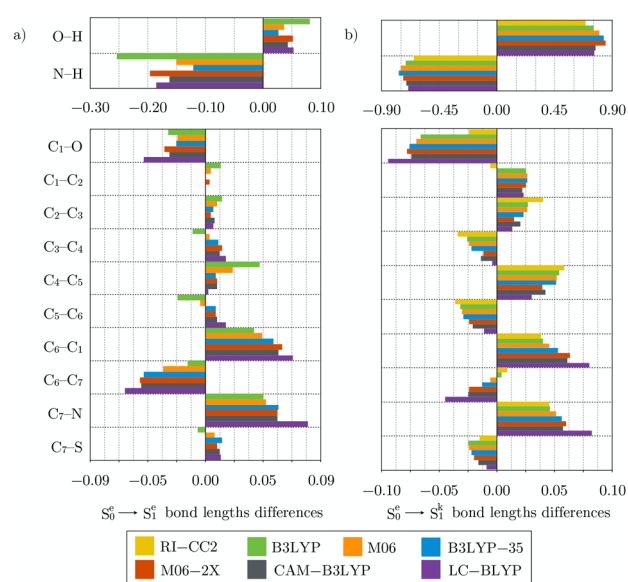


Figure 7. Bond lengths differences (in Å) going from (a) the enol ground state (S_0^e) to the enol excited state (S_1^e) ($\Delta = d(S_1^e) - d(S_0^e)$) and (b) the enol ground state (S_0^e) to the keto excited state (S_1^k) ($\Delta = d(S_1^k) - d(S_0^e)$) of 2-(2'-hydroxyphenyl)benzothiazole. See Figure 3 for atom numbering. Because no S_1^e minimum has been located for RI-CC2, the differences are reported with respect to the ground-state enol S_0^e .

decrease in N–H. The same is true for the C_1 – C_2 , C_2 – C_3 , and C_4 – C_5 bonds. In addition, B3LYP presents reduced C_3 – C_4 and C_5 – C_6 bond lengths with respect to the ground state, while for the other functionals an increase is observed (except for C_5 – C_6 with M06, presenting a small reduction). As a consequence of the reduction of the C_3 – C_4 and C_5 – C_6 bond lengths and of the increase in the C_2 – C_3 and C_4 – C_5 bonds observed for B3LYP and to a smaller extent for M06 XC functionals, their BLA values are large and negative contrary to the other XC functionals, where the values are also negative but small, comparable to those observed for the S_0^e form. Both C_6 – C_1 and C_6 – C_7 bond lengths, which are part of the six-membered ring from the OH group to the N atom, present the more pronounced changes among the C–C bonds upon excitation: C_6 – C_1 distances increase, while the C_6 – C_7 distances decrease. As shown by the variations of several bond lengths, the S_1^e structure is in between the S_0^e and S_1^k ones.

The bond length changes going from the S_0^e to the S_1^k minimum are presented in Figure 7b. Because the S_1^k minimum is not located at the RI-CC2 level, the differences are reported with respect to the ground-state *cis*-enol S_0^e . This S_1^k minimum is characterized by the transfer of the proton to the nitrogen, and so important reduction of the N–H distance and increase in the O–H one are observed. The biggest repercussion of the proton transfer is observed along the O– C_1 – C_6 – C_7 –N–H path: The C_1 –O and C_6 – C_7 bond lengths decrease, while the C_6 – C_1 and C_7 –N distances increase. The amplitude of these modifications is progressive when going from RI-CC2, B3LYP, M06, and B3LYP-35 until M06-2X. This is further evidenced by the increasing value of the $RMSD_6$. For M06-2X, the C_5 – C_6 – C_7 –N is different from the 180.0° value found for all of the other XC functionals, which explained the larger global $RMSD_{tot}$ value of 0.255 Å. These modifications indicate that the larger the amount of Hartree–Fock exchange the more keto-like is the structure with, for instance, a C_1 –O bond

Table 8. Representative Excited-State Bond Lengths (Å), Valence Angles and Dihedral Angles (degrees), and RMSD Values (Å) for 2-(2'-Hydroxyphenyl)benzothiazole^a

		RI-CC2	B3LYP	M06	B3LYP-35	M06-2X	CAM-B3LYP	LC-BLYP
S_1^s	C ₁ –O		1.311	1.308	1.315	1.304	1.308	1.295
	O–H		1.068	1.016	1.000	1.034	1.028	1.038
	N–H		1.496	1.631	1.667	1.567	1.581	1.542
	C ₁ –C ₂		1.410	1.398	1.395	1.400	1.394	1.386
	C ₂ –C ₃		1.395	1.384	1.384	1.383	1.382	1.372
	C ₃ –C ₄		1.387	1.395	1.403	1.408	1.403	1.401
	C ₄ –C ₅		1.422	1.395	1.384	1.386	1.383	1.367
	C ₅ –C ₆	—	1.382	1.394	1.409	1.407	1.406	1.404
	C ₆ –C ₁		1.456	1.455	1.465	1.470	1.465	1.464
	C ₆ –C ₇		1.439	1.416	1.408	1.407	1.405	1.389
	C ₇ –N		1.350	1.346	1.354	1.354	1.352	1.346
	C ₇ –S		1.761	1.767	1.775	1.761	1.762	1.742
	O–H–N		153.0	150.7	149.7	151.5	151.2	151.0
	C ₁ –O–H–N		0.0	0.0	0.0	0.0	0.0	0.0
	C ₅ –C ₆ –C ₇ –N		180.0	180.0	180.0	180.0	180.0	180.0
	C ₅ –C ₆ –C ₇ –S		0.0	0.0	0.0	0.0	0.0	0.0
	RMSD _{tot}		—	0.069	0.074	0.059	0.059	0.072
	RMSD ₆		—	0.044	0.057	0.025	0.030	0.023
	BLA _{C₁–C₆}			0.031	0.016	0.008	0.009	0.004
S_1^k	C ₁ –O	1.320	1.274	1.260	1.262	1.258	1.262	1.249
	O–H	1.685	1.739	1.777	1.805	1.829	1.755	1.743
	N–H	1.053	1.040	1.033	1.023	1.030	1.034	1.034
	C ₁ –C ₂	1.393	1.423	1.420	1.421	1.422	1.416	1.409
	C ₂ –C ₃	1.426	1.409	1.401	1.401	1.394	1.395	1.379
	C ₃ –C ₄	1.365	1.371	1.368	1.371	1.383	1.378	1.381
	C ₄ –C ₅	1.442	1.434	1.426	1.427	1.416	1.416	1.395
	C ₅ –C ₆	1.368	1.372	1.368	1.372	1.375	1.376	1.377
	C ₆ –C ₁	1.455	1.458	1.456	1.465	1.473	1.469	1.476
	C ₆ –C ₇	1.455	1.457	1.443	1.443	1.434	1.430	1.407
	C ₇ –N	1.368	1.351	1.350	1.353	1.358	1.353	1.348
	C ₇ –S	1.735	1.742	1.736	1.740	1.732	1.735	1.721
	O–H–N	139.7	136.8	134.7	133.7	130.5	134.7	133.6
	C ₁ –O–H–N	0.0	0.0	0.0	0.0	26.0	0.0	0.0
	C ₅ –C ₆ –C ₇ –N	180.0	180.0	180.0	180.0	157.3	180.0	180.0
	C ₅ –C ₆ –C ₇ –S	0.0	0.0	0.0	0.0	21.3	0.0	0.0
	RMSD _{tot}	—	0.026	0.021	0.025	0.255	0.020	0.041
	RMSD ₆	—	0.022	0.037	0.046	0.130	0.033	0.038
	BLA _{C₁–C₆}	–0.065	–0.045	–0.042	–0.043	–0.035	–0.037	–0.028
S_1^{wk}	C ₁ –O			1.244	1.240	1.231	1.237	
	O–H			3.307	3.351	3.563	3.532	
	N–H			1.005	0.999	1.007	1.005	
	C ₁ –C ₂			1.442	1.449	1.458	1.448	
	C ₂ –C ₃			1.368	1.365	1.357	1.357	
	C ₃ –C ₄			1.394	1.400	1.415	1.408	
	C ₄ –C ₅			1.406	1.403	1.387	1.385	
	C ₅ –C ₆	—	—	1.363	1.369	1.383	1.381	—
	C ₆ –C ₁			1.443	1.456	1.467	1.459	
	C ₆ –C ₇			1.484	1.482	1.468	1.468	
	C ₇ –N			1.384	1.390	1.398	1.397	
	C ₇ –S			1.728	1.737	1.739	1.736	
	O–H–N			81.8	78.0	76.0	88.0	
	C ₁ –O–H–N			88.9	89.1	73.1	72.3	
	C ₅ –C ₆ –C ₇ –N			98.6	99.6	75.8	77.4	
	C ₅ –C ₆ –C ₇ –S			100.7	100.7	69.5	70.9	
	RMSD _{tot}			—	0.021	0.441	0.410	
	BLA _{C₁–C₆}			–0.006	–0.002	0.015	0.012	

^aSee Figure 3 for atom numbering. RMSD values are evaluated with respect to B3LYP, RI-CC2, or M06 for S_1^s , S_1^k , or S_1^{wk} excited state, respectively.

Table 9. Vertical and Adiabatic Excitation Energies (eV) of 3-HC, SaOH, and HBT as Well as the Mean Difference with Respect to CC2

	RI-CC2	B3LYP	M06	B3LYP-35	M06-2X	CAM-B3LYP	LC-BLYP
				Vertical			
3-HC	4.17	3.99	4.10	4.37	4.29	4.44	4.72
SaOH	3.85	3.67	3.76	4.01	4.14	4.12	4.51
HBT	3.87	3.71	3.79	4.02	4.15	4.11	4.46
				Adiabatic			
3-HC	2.79	3.24	3.37	3.57	3.79	3.62	4.01
SaOH	—	2.89	3.01	3.16	3.35	3.30	3.61
HBT	3.21	3.26	3.37	3.50	3.67	3.61	3.87
mean Δ_{vert}	0.00	-0.17	-0.08	0.16	0.23	0.26	0.60
mean Δ_{adia}	0.00	0.25	0.37	0.53	0.73	0.62	0.94

length ranging from 1.27 (B3LYP) to 1.25 Å (LC-BLYP) for the different XC functionals in comparison with the 1.32 Å value obtained at the RI-CC2 level. The RI-CC2 geometry is therefore the most “enol-like” keto conformer with, for instance, a C₆–C₇ bond length that increases, while for all of the XC functionals (except B3LYP) the distance decreases. The benzene ring of the hydroxyphenyl part is also affected by the proton transfer. The different changes go in the same direction for all methods, except for the C₁–C₂ bond, for which RI-CC2 predicts a very small decrease, while all of the XC functionals indicate an increase in accordance with the Lewis structure of the keto form. Nevertheless, the alternation of single and double bonds in the benzene ring of the hydroxyphenyl moiety is not yet characteristic of a “pure” keto form, as already seen for the S₁^k form of *N*-salicylideneaniline molecule (the BLA values for the S₁^k forms of *N*-salicylideneaniline and 2-(2'-hydroxyphenyl)benzothiazole molecules are all negatives). Indeed, the BLA values of the S₁^k state are all negative and range from -0.028 to -0.065 Å, with the latter value found for RI-CC2. Negative BLA values indicate that the alternation is reversed with respect to the one in the keto product (S₀^k), as illustrated in the Lewis structure for the S₁^k state in Figure 3. At last, at the RI-CC2 level, the hydrogen-bonding character is stronger, as demonstrated by the N–H and O–H distances that are the longest and the shortest, respectively, compared with what is obtained at the TDDFT level of theory.

At last, the twisted-keto S₁^{twk} conformer is only found using four XC functionals, probably due to the proximity of the conical intersection: M06, B3LYP-35, M06-2X, and CAM-B3LYP. With respect to the S₁^k equilibrium geometry, the twisted-keto S₁^{twk} form presents a rotation of the hydroxyphenyl group around the C₆–C₇ bond. The amplitude of this rotation varies with the XC functional: M06 and B3LYP-35 present a dihedral angle of ~100° between both C₅–C₆–C₇–N and C₅–C₆–C₇–S path, while these angles are closer to 70° for M06-2X and CAM-B3LYP and present a difference of 6° between the two paths, which indicates a small pyramidalization of the thiazole ring. With the rotation, the H-bonded character is reduced, leading to a reduction of the C₁–O bond length as well as a reduction of the N–H distance.

FURTHER DISCUSSION AND CONCLUSIONS

To understand the processes that take place during photoexcitation, it is of crucial importance to characterize the structures and energies of the involved electronic excited states using appropriate quantum-chemistry methods. This work presents a first step toward this goal by investigating the energy minima on the potential energy surfaces of the ground and

excited states of three photoactive molecules that undergo intramolecular proton transfer in the excited state: 3-hydroxychromone (3-HC), *N*-salicylideneaniline (SaOH), and 2-(2'-hydroxyphenyl)benzothiazole (HBT). We have used the RI-CC2 method as well as the TDDFT methodology together with different exchange–correlation (XC) functionals containing various percentages of Hartree–Fock exchange. This choice of the XC functionals originates from the well-known impact of the HF exchange on the charge-transfer excitation energies^{13–16,19} and oscillator strengths.^{31,32} Besides the comparative analysis of the structures along the reaction paths, this study has compared the TDDFT and CC2 results to provide guidelines for selecting the “best” XC functionals.

First, from the TDDFT vertical excitation energies, one observes that the M06 and B3LYP-35 values (Table 9) are in good agreement with those obtained at the RI-CC2 level of theory. Moreover, in agreement with previous investigations, the TDDFT vertical excitation energies increase with the amount of Hartree–Fock exchange. Then, this study has systematically addressed the ground-state geometries, those of the excited states, and their variations upon excitation. In general, for the ground state, the different methods provide similar geometries, as highlighted by small RMSD values. The major discrepancies are related to the hydrogen bonds, which are systematically stronger (shorter) at the RI-CC2 level than with the TDDFT methods. In addition, for the S₀^k form of the *N*-salicylideneaniline molecule, we have observed larger RMSD values, which are explained by large differences in the C₇–N–C₈–C₉ torsion angle.

The situation is different for the excited states. First, not all methods/XC functionals locate the same number of minima. For instance, for HBT molecule, the S₁^{twk} minimum that is close to a conical intersection is only found at the TDDFT level with the M06, B3LYP-35, M06-2X, and CAM-B3LYP XC functionals. Second, the geometrical parameters for the excited state obtained at the TDDFT level are more different from those obtained with the RI-CC2 method than what was observed for ground states. For instance, for HBT molecule, the changes of C₁–C₂ and C₆–C₇ bond lengths upon S₀^c → S₁^k electronic excitation are reversed for RI-CC2 in comparison with the TDDFT ones. This has repercussions on the bond length alternation (BLA) of the “phenol” ring (the smaller the BLA, the more aromatic the phenol ring) and in the hydrogen-bonding network. In particular, when analyzing the BLA values for SaOH and HBT molecules, we have observed that (1) for both S₀^c forms, the BLA values are very close to zero, indicating a good π -electron delocalization in the ring, and (2) for the S₀^c form and the two S₀^{twk} minima, the BLA values are positive while

they are negative for the S_k^k forms, indicating a reversed alternation of single and double bonds. In addition, several geometrical parameters vary monotonically with the amount of Hartree–Fock exchange (O–H, N–H, and C_1 – C_2 bond lengths for HBT molecule, for instance). This is also observed when analyzing the changes of the geometrical parameters upon excitation.

In conclusion, for the three systems investigated here, the M06 XC functional seems to best reproduce the RI-CC2 reference results. Still, RI-CC2 presents for the excited keto geometry a more “enol-like” structure, while TDDFT/M06 gives a more “keto-like” geometry. Following these conclusions, we can expect even larger effects of the methods on the spectroscopic signatures.

AUTHOR INFORMATION

Corresponding Author

*E-mail: vincent.liegeois@unamur.be.

ORCID

Benoît Champagne: 0000-0003-3678-8875

Vincent Liégeois: 0000-0003-2919-8025

Notes

The authors declare no competing financial interest.

ACKNOWLEDGMENTS

This work was supported by funds from the Belgian Government (IUAP No P7/5 “Functional Supramolecular Systems”). O.L. thanks the Belgian Government under IUAP for his doctoral grant. V.L. thanks the Fund for Scientific Research (FRS-FNRS) for his Research Associate position. The calculations were performed on the computing facilities of the Consortium des Équipements de Calcul Intensif (CÉCI, <http://www.ceci-hpc.be>), particularly those of the Technological Platform of High Performance Computing, for which we gratefully acknowledge the financial support of the FNRS-FNRC (Conventions 2.4.617.07.F and 2.5020.11) and of the University of Namur.

REFERENCES

- (1) Towrie, M.; Doorley, G. W.; George, M. W.; Parker, A. W.; Quinn, S. J.; Kelly, J. M. ps-TRIR covers all the bases – recent advances in the use of transient IR for the detection of short-lived species in nucleic acids. *Analyst* **2009**, *134*, 1265–1273.
- (2) Kukura, P.; McCamant, D. W.; Mathies, R. A. Femtosecond stimulated Raman spectroscopy. *Annu. Rev. Phys. Chem.* **2007**, *58*, 461–488.
- (3) Elsaesser, T.; Kaiser, W. Visible and infrared spectroscopy of intramolecular proton transfer using picosecond laser pulses. *Chem. Phys. Lett.* **1986**, *128*, 231–237.
- (4) Fang, C.; Frontiera, R. R.; Tran, R.; Mathies, R. A. Mapping GFP structure evolution during proton transfer with femtosecond Raman spectroscopy. *Nature* **2009**, *462*, 200–204.
- (5) Liu, W.; Han, F.; Smith, C.; Fang, C. Ultrafast conformational dynamics of pyranine during excited state proton transfer in aqueous solution revealed by femtosecond stimulated Raman spectroscopy. *J. Phys. Chem. B* **2012**, *116*, 10535–10550.
- (6) Han, F.; Liu, W.; Fang, C. Excited-state proton transfer of photoexcited pyranine in water observed by femtosecond stimulated Raman spectroscopy. *Chem. Phys.* **2013**, *422*, 204–219.
- (7) Wnuk, P.; Burdziński, G.; Sliwa, M.; Kijak, M.; Grabowska, A.; Sepiol, J.; Kubicki, J. From ultrafast events to equilibrium-uncovering the unusual dynamics of ESIPT reaction: The case of dually fluorescent diethyl-2,5-(dibenzoxazolyl)-hydroquinone. *Phys. Chem. Chem. Phys.* **2014**, *16*, 2542–2552.
- (8) Perrier, A.; Aloise, S.; Pawlowska, Z.; Sliwa, M.; Maurel, F.; Abe, J. Photoinduced intramolecular charge transfer process of betaine pyridinium: A theoretical spectroscopic study. *Chem. Phys. Lett.* **2011**, *515*, 42–48.
- (9) Kukura, P.; McCamant, D. W.; Yoon, S.; Wandschneider, D. B.; Mathies, R. A. Structural observation of the primary isomerization in vision with femtosecond-stimulated Raman. *Science* **2005**, *310*, 1006–1009.
- (10) Nibbering, E. T. J.; Fidler, H.; Pines, E. Ultrafast chemistry: Using time-resolved vibrational spectroscopy for interrogation of structural dynamics. *Annu. Rev. Phys. Chem.* **2005**, *56*, 337–367.
- (11) Koch, W.; Holthausen, M. C. *A Chemist's Guide to Density Functional Theory*; Wiley-VCH Verlag GmbH: Weinheim, Germany, 2001.
- (12) Runge, E.; Gross, E. K. U. Density-Functional Theory for Time-Dependent Systems. *Phys. Rev. Lett.* **1984**, *52*, 997.
- (13) Tozer, D. J. Relationship between long-range charge-transfer excitation energy error and integer discontinuity in Kohn-Sham theory. *J. Chem. Phys.* **2003**, *119*, 12697–12699.
- (14) Dreuw, A.; Weisman, J. L.; Head-Gordon, M. Long-range charge-transfer excited states in time-dependent density functional theory require non-local exchange. *J. Chem. Phys.* **2003**, *119*, 2943.
- (15) Guillaume, M.; Champagne, B.; Zutterman, F. Investigation of the UV/visible absorption spectra of merocyanine dyes using time-dependent density functional theory. *J. Phys. Chem. A* **2006**, *110*, 13007–13013.
- (16) Grimme, S.; Neese, F. Double-hybrid density functional theory for excited electronic states of molecules. *J. Chem. Phys.* **2007**, *127*, 154116.
- (17) Laurent, A. D.; Jacquemin, D. TD-DFT benchmarks: A review. *Int. J. Quantum Chem.* **2013**, *113*, 2019–2039.
- (18) Adamo, C.; Jacquemin, D. The calculations of excited-state properties with time-dependent density functional theory. *Chem. Soc. Rev.* **2013**, *42*, 845–856.
- (19) Champagne, B.; Liégeois, V.; Zutterman, F. Pigment violet 19 – a test case to define a simple method to simulate the vibronic structure of absorption spectra of organic pigments and dyes in solution. *Photochem. Photobiol. Sci.* **2015**, *14*, 444–456.
- (20) Lyakh, D. I.; Musiał, M.; Lotrich, V. F.; Bartlett, R. J. Multireference nature of chemistry: The coupled-cluster view. *Chem. Rev.* **2012**, *112*, 182–243.
- (21) Christiansen, O.; Koch, H.; Jørgensen, P. The second-order approximate coupled cluster singles and doubles model CC2. *Chem. Phys. Lett.* **1995**, *243*, 409–418.
- (22) Quartarolo, A. D.; Russo, N. A Computational Study (TDDFT and RIC2) of the Electronic Spectra of Pyranoanthocyanins in the Gas Phase and Solution. *J. Chem. Theory Comput.* **2011**, *7*, 1073–1081.
- (23) Graf, N. K.; Friese, D. H.; Winter, N. O. C.; Hättig, C. Excited state polarizabilities for CC2 using the resolution-of-the-identity approximation. *J. Chem. Phys.* **2015**, *143*, 244108.
- (24) Jacquemin, D. Excited-State Dipole and Quadrupole Moments: TD-DFT versus CC2. *J. Chem. Theory Comput.* **2016**, *12*, 3993–4003.
- (25) Vahtras, O.; Almlöf, J.; Feyereisen, M. W. Integral approximations for LCAO-SCF calculations. *Chem. Phys. Lett.* **1993**, *213*, 514–518.
- (26) Sliwa, M.; Mouton, N.; Ruckebusch, C.; Poisson, L.; Idrissi, A.; Aloise, S.; Potier, L.; Dubois, J.; Poizat, O.; Buntinx, G. Investigation of ultrafast photoinduced processes for salicylidene aniline in solution and gas phase: toward a general photo-dynamical scheme. *Photochem. Photobiol. Sci.* **2010**, *9*, 661–669.
- (27) Ruckebusch, C.; Sliwa, M.; Pernot, P.; de Juan, A.; Tauler, R. Comprehensive data analysis of femtosecond transient absorption spectra: A review. *J. Photochem. Photobiol., C* **2012**, *13*, 1–27.
- (28) Lochbrunner, S.; Wurzer, A. J.; Riedle, E. Microscopic mechanism of ultrafast excited-state intramolecular proton transfer: A 30-fs study of 2-(2'-hydroxyphenyl)benzothiazole. *J. Phys. Chem. A* **2003**, *107*, 10580–10590.
- (29) Barbatti, M.; Aquino, A. J. A.; Lischka, H.; Schriever, C.; Lochbrunner, S.; Riedle, E. Ultrafast internal conversion pathway and

mechanism in 2-(2'-hydroxyphenyl)benzothiazole: A case study for excited-state intramolecular proton transfer systems. *Phys. Chem. Chem. Phys.* **2009**, *11*, 1406–1415.

(30) Chevalier, K.; Grün, A.; Stamm, A.; Schmitt, Y.; Gerhards, M.; Diller, R. ESIP and Photodissociation of 3-Hydroxychromone in Solution: Photoinduced Processes Studied by Static and Time-Resolved UV/Vis, Fluorescence, and IR Spectroscopy. *J. Phys. Chem. A* **2013**, *117*, 11233–11245.

(31) Miura, M.; Aoki, Y.; Champagne, B. Assessment of time-dependent density functional schemes for computing the oscillator strengths of benzene, phenol, aniline, and fluorobenzene. *J. Chem. Phys.* **2007**, *127*, 084103.

(32) Silva-Junior, M. R.; Schreiber, M.; Sauer, S. P. A.; Thiel, W. Benchmarks for electronically excited states: time-dependent density functional theory and density functional theory based multireference configuration interaction. *J. Chem. Phys.* **2008**, *129*, 104103.

(33) TURBOMOLE, V6.0.2 2009; University of Karlsruhe and Forschungszentrum Karlsruhe GmbH, 1989–2007, TURBOMOLE GmbH, Since 2007.

(34) Frisch, M. J.; Trucks, G. W.; Schlegel, H. B.; Scuseria, G. E.; Robb, M. A.; Cheeseman, J. R.; Scalmani, G.; Barone, V.; Mennucci, B.; Petersson, G. A.; et al. *Gaussian 09*, revision D.01; Gaussian, Inc.: Wallingford, CT, 2009.

(35) Becke, A. D. Density-functional thermochemistry. III. The role of exact exchange. *J. Chem. Phys.* **1993**, *98*, 5648–5652.

(36) Zhao, Y.; Truhlar, D. G. The M06 suite of density functionals for main group thermochemistry, thermochemical kinetics, non-covalent interactions, excited states, and transition elements: Two new functionals and systematic testing of four M06-class functionals and 12 other functionals. *Theor. Chem. Acc.* **2008**, *120*, 215–241.

(37) Iikura, H.; Tsuneda, T.; Yanai, T.; Hirao, K. A long-range correction scheme for generalized-gradient-approximation exchange functionals. *J. Chem. Phys.* **2001**, *115*, 3540.

(38) Yanai, T.; Tew, D.; Handy, N. C. A new hybrid exchange-correlation functional using the Coulomb-attenuating method (CAM-B3LYP). *Chem. Phys. Lett.* **2004**, *393*, 51–57.

(39) Weigend, F.; Ahlrichs, R. Balanced Basis Sets of Split Valence, Triple Zeta Valence and Quadruple Zeta Valence Quality for H to Rn: Design and Assessment of Accuracy. *Phys. Chem. Chem. Phys.* **2005**, *7*, 3297.

(40) Weigend, F.; Häser, M.; Patzelt, H.; Ahlrichs, R. RI-MP2: optimized auxiliary basis sets and demonstration of efficiency. *Chem. Phys. Lett.* **1998**, *294*, 143–152.

(41) Horn, B. K. P. Closed-form solution of absolute orientation using unit quaternions. *J. Opt. Soc. Am. A* **1987**, *4*, 629–642.

(42) Coutsiaris, E. A.; Seok, C.; Dill, K. Using quaternions to calculate RMSD. *J. Comput. Chem.* **2004**, *25*, 1849–1857.

(43) Perveaux, A.; Lorphelin, M.; Lasorne, B.; Lauvergnat, D. Fast and slow excited-state intramolecular proton transfer in 3-hydroxychromone: a two-state story? *Phys. Chem. Chem. Phys.* **2017**, *19*, 6579–6593.